



1980 N. Atlantic Ave., Suite 230
Coca Beach, FL 32931
(321) 783-9735, (321) 853-8202 (AMU)

Applied Meteorology Unit (AMU) Quarterly Report



Third Quarter FY-04

Contract NAS10-01052

31 July 2004

Distribution:

NASA HQ/MF. Gregory
 NASA KSC/AA/J. Kennedy
 NASA KSC/MK/D. Kross
 NASA KSC/PH/ M. Wetmore
 NASA KSC/PH-A2/D. Lyons
 NASA KSC/PH/M. Leinbach
 NASA KSC/PH/S. Minute
 NASA KSC/PH-A/J. Guidi
 NASA KSC/YA/J. Heald
 NASA KSC/YA-C/D. Bartine
 NASA KSC/YA-D/G. Clements
 NASA KSC/YA-D/J. Madura
 NASA KSC/YA-D/F. Merceret
 NASA JSC/MA/W. Parsons
 NASA JSC/MS2/C. Boykin
 NASA JSC/ZS8/F. Brody
 NASA JSC/ZS8/R. Lafosse
 NASA JSC/ZS8/B. Hoeth
 NASA MSFC/ED41/W. Vaughan
 NASA MSFC/ED44/D. Johnson
 NASA MSFC/ED44/B. Roberts
 NASA MSFC/ED44/S. Deaton
 NASA MSFC/MP71/S. Glover
 NASA DFRC/RA/J. Ehemberger
 45 WS/CC/R. LaFebre
 45 WS/DO/P. Broll
 45 WS/DOR/T. McNamara
 45 WS/DOR/J. Moffitt
 45 WS/DOR/J. Tumbiolo
 45 WS/DOR/K. Winters
 45 WS/DOR/J. Weems
 45 WS/SY/D. Hajek
 45 WS/SY/A/B. Boyd
 45 WS/SY/O/F. Flinn
 45 WS/SYR/W. Roeder
 45 MXG/CC/B. Presley
 45 MXG/LGP/R. Fore
 45 SW/SESL/D. Berlinrut
 45 OG/CC/G. Billman
 CSR 4140/H. Herring
 CSR 7000/M. Maier
 SMC/RNP/D. Salm
 SMC/RNP/T. Knox
 SMC/RNP/R. Bailey
 SMC/RNP (PRC)/P. Conant
 HQ AFSPC/XOSW/A. Gibbs
 HQ AFWA/CC/C. Benson
 HQ AFWA/DNX/W. Cade
 HQ AFWA/DN/M. Zettlemoyer
 HQ USAF/XOW/R. Clayton
 HQ USAF/XOWX/J. Lanicci
 NOAA "W/NP"/L. Uccellini
 NOAA/OAR/SSMC-I/J. Golden
 NOAA/NWS/OST12/SSMC2/J. McQueen
 NOAA Office of Military Affairs/N. Wyse
 NWS Melbourne/B. Hagemeyer
 NWS Southern Region HQ/"W/SRH"/
 X. W. Proenza
 NWS Southern Region HQ/"W/SR3"/
 D. Smith
 NWS/"W/OST1"/B. Saffie
 NWS/"W/OST12"/D. Melendez
 NSSL/D. Forsyth
 NSSL/C. Crisp
 30 WS/SY/M. Schmeiser
 30 WS/SYR/L. Wells
 30 WS/CC/C. Keith
 30 WS/DO/S. Saul
 30 SW/XPE/R. Ruecker

Continued on Page 2

Executive Summary

This report summarizes the Applied Meteorology Unit (AMU) activities for the third quarter of Fiscal Year 2004 (April - June 2004). A detailed project schedule is included in the Appendix.

Task Objective Lightning Probability Forecast: Phase I

Goal Develop a set of statistical equations to forecast the probability of lightning occurrence for the day. This will aid forecasters in evaluating flight rules and determining the probability of launch commit criteria violations, as well as preparing forecasts for ground operations.

Milestones Tables showing the probabilities of lightning occurrence based on flow regime were distributed to the forecasters at the 45th Weather Squadron (45 WS), Spaceflight Meteorology Group (SMG), and the National Weather Service office at Melbourne FL (NWS MLB).

Discussion Preparation of predictors for the equation development began, starting with determination of lightning occurrence probabilities for the six different flow regimes. Probabilities were the highest for southwest flow in all warm season months, reaching 79% in June, July, and August.

Task Mesonet Temperature and Wind Climatology

Goal Identify biases in the wind and temperature observations at individual or groups of sensors based on location, weather conditions, and sensor exposure. Any deviations in the data field could adversely affect forecasts and analyses for ground, launch, and landing operations.

Milestones A draft of the final report was completed and is currently in the customer review process. The graphical user interface (GUI) tool for displaying the climatology results was also completed this past quarter.

Discussion A sample of tower climatology results from the final report illustrates some of the typical characteristics of wind speeds across the Kennedy Space Center (KSC) and Cape Canaveral Air Force Station (CCAFS).

Task Severe Weather Forecast Decision Aid

Goal Create a new forecast aid to improve the severe weather watches and warnings for the protection of KSC/CCAFS personnel and property.

Milestones The database of severe weather events was expanded to include an archive at the Storm Prediction Center and synoptic weather patterns. Stability indices were calculated from CCAFS soundings between 0900 – 1100 UTC to provide data for days without a 1000 UTC sounding.

Discussion Initial findings show that stability indices are not representative of days with versus those without reported severe weather. A further breakout of the non-severe days into thunderstorm/non-thunderstorm days will be investigated, and then indices from the non-reported severe thunderstorm days will be compared to severe weather days.

Continued on Page 2

Distribution (continued from Page 1)

88 WS/WES/K. Lehneis
 88 WS/WES/G. Marx
 46 WS//DO/M. Treu
 46 WS/WST/A. Michels
 412 OSS/OSWM/P. Harvey
 FSU Department of Meteorology/P. Ray
 FSU Department of Meteorology/H. Fuelberg
 NCAR/J. Wilson
 NCAR/Y. H. Kuo
 NOAA/ERL/FSL/J. McGinley
 Office of the Federal Coordinator for Meteorological Services and Supporting Research/J. Harrison, R. Dumont
 Boeing Houston/S. Gonzalez
 Aerospace Corp/T. Adang
 ACTA, Inc./B. Parks
 ENSCO, Inc./T. Wilfong
 ENSCO, Inc./E. Lambert

**TABLE
of
CONTENTS**

**SHORT-TERM FORECAST
IMPROVEMENT**

Objective Lightning
Probability 3

Mesonet Temperature and
Wind Climatology 6

Severe Weather Forecast
Decision Aid 10

Shuttle Ascent Camera
Cloud Obstruction Forecast
..... 13

**INSTRUMENTATION AND
MEASUREMENT**

I&M and RSA Support ... 14

Anvil Transparency
Relationship to Radar
Reflectivity 14

MESOSCALE MODELING

User Control Interface for
ADAS Data Ingest 17

**AMU CHIEF'S
TECHNICAL ACTIVITIES**
..... 17

AMU OPERATIONS 18

REFERENCES 18

LIST OF ACRONYMS... 19

APPENDIX A 20

Executive Summary, *continued*

Task Shuttle Ascent Camera Cloud Obstruction Forecast

Goal In response to a request from the Shuttle Program to implement a recommendation of the Columbia Accident Investigation Board, develop a model to forecast the probability that at least three of the shuttle ascent imaging cameras will have a view of the shuttle launch vehicle unobstructed by cloud at any time from launch to Solid Rocket Booster separation.

Milestones Computer simulations and analyses of viewing probabilities were completed and a draft final report is being reviewed. The results from the simulations were briefed to the Shuttle Launch Director and an Integration Control Board. Additional briefings are scheduled for July.

Discussion As reported in the final report, there was a significant improvement in the viewing probabilities with the new proposed camera network upgrade, especially when two airborne cameras are included. The final report will also include the sensitivity of viewing probabilities to cloud height, thickness, size and layering.

Task Anvil Transparency Relationship to Radar Reflectivity

Goal Determine if products from the NWS MLB WSR-88D radar can be used to analyze anvil cloud transparency, an important element in forecasting launch commit criteria. Opaque anvils can carry an electrical charge. If a vehicle flies through such a charge, it could trigger lightning and be destroyed.

Milestones A total of 313 hours of radar products were compared with surface observations of opaque and transparent anvil clouds. A draft memorandum describing the results of the comparison was completed and forwarded to SMG and the 45 WS for their comments.

Discussion The radar products showed some utility in detecting opaque anvil clouds with a probability of detection of ~ 50% and a false alarm rate of ~ 10%. When the radar data indicates an anvil cloud exists, there is a high probability that it is opaque. When there is no indication of anvil clouds in the radar data, there is a 50% probability that the anvil clouds are opaque.

Task User Control Interface for ADAS Data Ingest

Goal Develop a GUI to help forecasters manage the data sets assimilated into the operational Advanced Regional Prediction System (ARPS) Data Analysis System (ADAS) run at NWS MLB and SMG.

Milestones Met with NWS MLB personnel to collaborate on a framework for designing a control GUI for forecaster use and developed the initial layout of a menu-driven GUI and interactive quality-control map.

Discussion One of ENSCO's software engineers, Mr. Jeremy Keen, is developing the control GUI. He will work closely with the Mr. Case and AMU customers to develop, test, and implement the features of interest for the ADAS control GUI.

Special Notice to Readers

Applied Meteorology Unit (AMU) Quarterly Reports are now available on the Wide World Web (WWW) at <http://science.ksc.nasa.gov/amu/>.

The AMU Quarterly Reports are also available in electronic format via email. If you would like to be added to the email distribution list, please contact Ms. Winifred Lambert (321-853-8130, lambert.winifred@ensco.com). If your mailing information changes or if you would like to be removed from the distribution list, please notify Ms. Lambert or Dr. Francis Merceret (321-867-0818, Francis.J.Merceret@nasa.gov).

Background

The AMU has been in operation since September 1991. Tasking is determined annually with reviews at least semi-annually. The progress being made in each task is discussed in this report with the primary AMU point of contact reflected on each task.

AMU ACCOMPLISHMENTS DURING THE PAST QUARTER

SHORT-TERM FORECAST IMPROVEMENT

Objective Lightning Probability: Phase I (Ms. Lambert and Mr. Wheeler)

The 45th Weather Squadron (45 WS) forecasters include a probability of thunderstorm occurrence in their daily morning briefings. This information is used by personnel involved in determining the possibility of violating Launch Commit Criteria (LCC), evaluating Flight Rules (FR), and daily planning for ground operation activities on Kennedy Space Center/Cape Canaveral Air Force Station (KSC/CCAFS). Much of the current lightning probability forecast is based on a subjective analysis of model and observational data. The forecasters requested that a lightning probability forecast tool based on statistical analysis of historical warm-season data be developed. Such a tool would increase the objectivity of the daily thunderstorm probability forecast. The AMU is developing statistical lightning forecast equations that will provide a lightning occurrence probability for the day by 1100 UTC (0700 EDT) during the months May – September (warm season). The tool will be based on the results from several research projects. If tests of the equations show that they improve the daily lightning forecast, the AMU will develop a

PC-based tool from which the daily probabilities can be displayed by the forecasters. The three data types to be used in this task were described in previous AMU Quarterly Reports (Q4 FY03 and Q1 FY04):

- Cloud-to-Ground Lightning Surveillance System (CGLSS) data,
- 1200 UTC sounding data from synoptic sites in Florida, and
- 1000 UTC CCAFS sounding (XMR) data.

Ms. Lambert is using the S-PLUS[®] software package (Insightful Corporation 2000) to process and analyze the data, and to develop the lightning forecast equations.

Flow Regime Predictor

One of the predictors that Ms. Lambert will use in the equation development is the daily peninsular-scale flow regime as described in Lericos et al. (2002). The 45 WS asked Ms. Lambert to determine the probability of lightning occurrence over KSC/CCAFS based on flow regime, and to provide tables of the probability values for operational use. The probabilities were calculated using the CGLSS data and the daily flow regimes determined by the height-weighted average wind direction using all observations (mandatory and significant) in the 1000 – 700 mb layer from the Miami (MIA), Tampa (TBW), and

Jacksonville (JAX) FL 1200 UTC soundings. The data are from all warm seasons during the years 1989 – 2003, and the time period for lightning occurrence on each day is 0700 – 2400 EDT. Some statistics that describe the number of lightning strikes associated with each regime were also calculated.

Working closely with Mr. Roeder of the 45 WS to ensure the tables would be useful to

operations, Ms. Lambert created one table for the entire warm season and a table for each individual month: six tables in all. Each table has a descriptive caption at the top, six columns and a notes section at the bottom.

The table below provides an example of the content in all the tables. It contains the lightning statistics by flow regime for the entire warm season.

Flow Regime Lightning Statistics Warm Season (May – September) 1989 – 2003					
Probabilities of lightning occurring within a rectangle encompassing all 5 n mi warning rings based on flow regime are shown in the right-most column.					
The strikes/day statistical values in the second column are based on lightning days only (fifth column). The median (M) value of strikes per day in each regime is shown with the 1st (Q1) and 3rd (Q3) quantiles in the order Q1, M, Q3. The mean and standard deviation of the strike numbers are shown in parentheses below Q1, M, Q3 (see explanation of M, Q1, and Q3 below).					
<i>Flow Regime</i>	<i>Q1, M, Q3 of Strikes/Day (Mean, Stdev)</i>	<i>Total # Days (% of Total)</i>	<i># Non Lightning Days</i>	<i># Lightning Days</i>	<i>Probability of Lightning</i>
SW-1 Ridge S of MIA	68, 248, 507 (396, 496)	271 (12.7)	92	179	66 %
SW-2 Ridge between MIA/TBW	37, 169, 528 (357, 435)	218 (10.2)	60	158	72 %
SE-1 Ridge between TBW/JAX	4, 18, 110 (117, 223)	283 (13.3)	140	143	51 %
SE-2 Ridge N of JAX	3, 8, 41 (61,141)	218 (10.2)	133	85	39 %
NW	28, 179, 359 (342, 545)	93 (4.4)	53	40	43 %
NE	2, 14, 62 (68, 114)	100 (4.7)	82	18	18 %
Other (Regime Undefined)	9, 65, 265 (200, 325)	945 (44.4)	527	418	44 %
TOTALS	10, 75, 324 (238, 381)	2128	1087	1041	49 %
There is a 6% improvement in the forecast when using the individual flow regime probabilities over the seasonal climatological probability of 49%, and a 23% improvement over 1-day persistence. Forecast improvement was calculated using the Brier Skill Score.					
The median is the strike-number value at which 50% of the cases had higher and 50% had lower strike numbers, i.e. the center of the strike-number distribution. It is <i>not</i> equal to the mean because the strike-number distributions are not symmetric. The 'middle' 50% of the cases are found between Q1 and Q3. For asymmetric distributions, like lightning strikes/day, the median and inter-quartile range are more representative of the data than the mean and standard deviation.					

The first column contains the names of the flow regimes as defined in Lericos et al. (2002). The acronyms are standard for wind directions: southwest (SW), southeast (SE), northwest (NW), and (NE). The first four regimes are dependent on the location of the subtropical ridge that is usually present during the warm season, resulting in two SW and two SE regimes. The Other classification was used for days in which the regime did not fit in the other six categories. The Totals row shows the statistical properties of all flow regimes combined.

The second column contains statistics that show the properties of the strike counts for days on which lightning occurred in each flow regime. The first line in the cell shows the first quantile, median, and third quantile of the daily strike numbers. The second line in the cell contains the mean and standard deviation values in parentheses. Means and standard deviations are used for describing distributions that are Gaussian (symmetric). For most of the cases in the above table, the standard deviation of the strikes per day is larger than the mean. This would result in a negative value for the first standard deviation below the mean. While this is possible for Gaussian distributions in general, it is not possible for these data since there cannot be a negative number of lightning strikes. A larger standard deviation indicates that the distribution of the daily strike numbers is not symmetric. For asymmetric distributions, the median and quartiles are more representative of the data distribution than mean and standard deviation.

The third column shows the number of days that each flow regime occurred during the period. The number in parenthesis to the right is the percentage of days that flow regime occurred in the period. The fourth column shows the subset of flow regime days on which lightning did not occur, and conversely the fifth column shows the number of days on which lightning occurred.

The value in the sixth (right-most) column is the climatological probability of lightning occurrence based on flow regime, and was calculated by dividing the number of lightning days (Column 5) by the total number of flow regime days (Column 3) and multiplying by 100. This value can be used by forecasters, along with all other available tools, as an aid to daily probabilistic thunderstorm and lightning forecasting.

There is further information found in the notes in the last row of the table. The second note gives

a brief description of median and first and third quantiles of the daily strike numbers. The first paragraph describes the forecast performance of the flow regime lightning probabilities when compared to that of climatology and 1-day persistence in terms of percent forecast improvement or degradation. The value is calculated through a set of two equations. The first is the Brier Score (BS) calculation (Wilks 1995), and is the mean-squared error of the probability forecasts (p) considering that the observation value (o) is 1 when lightning occurred and 0 when it did not. The BS averages the squared differences between pairs of probability forecasts and binary observations:

$$BS = \frac{1}{n} \sum_{i=1}^n (p_i - o_i)^2, \quad (1)$$

where n is the number of forecast/observation pairs and i is the index of the individual pairs in the set.

The probabilities of lightning were considered the probability forecasts. The 45 WS was interested in how well the flow regime probabilities performed as forecasts compared to a climatological probability forecast and 1-day persistence. The climatology forecast was the probability value in the Totals row, which is the overall climatological probability value for the time period in the table. The 1-day persistence forecast was binary (0 or 1), just like the observations. It assumed that whatever occurred on one day also occurred on the following day. The BS for each of these forecast methods were calculated and used in the Brier Skill Score (SS) equation to calculate the relative improvement in the forecast:

$$SS = \frac{BS - BS_{ref}}{BS_{perfect} - BS_{ref}}, \quad (2)$$

where BS is the Brier Score of the probability forecast being tested, BS_{ref} is the reference or benchmark forecast, and $BS_{perfect}$ is the Brier Score of a perfect forecast, which is always 0 (see Equation 1).

The flow regime probabilities were used for BS in Equation 2, and the climatological probability and 1-day persistence values were used for BS_{ref} . Two SS values were calculated: one for the comparison between the flow regime probabilities and climatology, and the other between the flow regime probabilities and 1-day persistence. In every case, use of the flow regime probabilities produced an improvement in the forecast over climatology and 1-day persistence.

diurnal speed distributions except for October through January. Nighttime wind speeds were higher at coastal tower 0022 compared to the causeway tower, particularly in October, when east - northeasterly winds tended to occur more frequently than other directions (not shown). The predominance of northeasterly wind directions led to stronger winds along the immediate coast compared to the causeway tower, because of the frictional effects as winds cross the land mass upstream of Tower 0300.

Towers 0509 and 0819 show further how the average wind speeds can vary between the coast and Merritt Island and the mainland, respectively. The average speeds decrease with distance from the coast in these stations due to frictional effects from land masses surrounding these towers. The average wind speed for all the towers lies in between the averages of the coastal, Merritt Island, and mainland towers. This illustrates that an overall mean wind is not representative of the individual towers in the network.

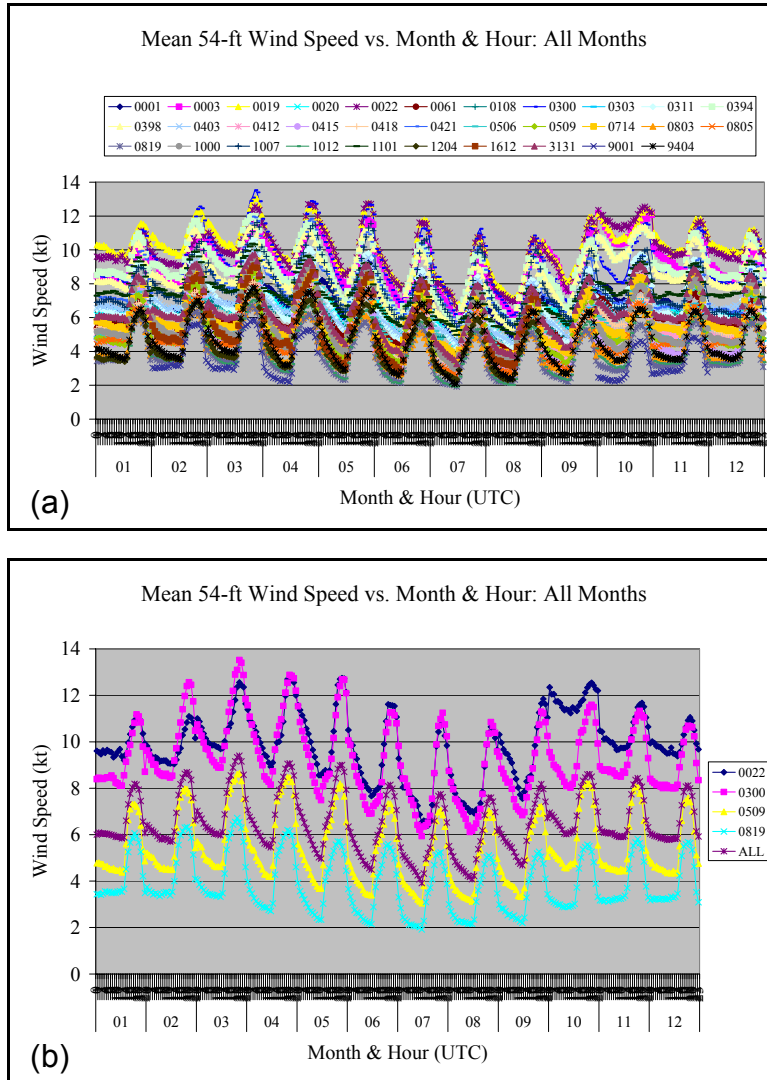


Figure 2. Hourly mean wind speeds for all months of the year at (a) all towers, and (b) towers 0022, 0300, 0509, 0819, and all towers averaged together (ALL). The hourly values by month are along the x-axis. The months are represented by their numerical value, and the individual hours in each month are difficult to discern because they are very close together on the axis.

During the winter months, the time of the maximum mean speed corresponds well with the time of maximum heating. In the spring and summer months when daily sea breezes predominate, the time of maximum speeds are delayed by a few hours after peak heating. These relationships are illustrated in Figure 3, which shows an overlay of the hourly mean temperature differences between the near-shore buoy 41009 (T_b) and the overall tower network average 6-ft temperature (T_n), and the mean wind speed normalized by the monthly mean value (all-mean). This normalization is done by subtracting each month's overall mean speed from the individual hourly mean wind speed, in order to have similar scales along the y-axis for easier comparison. Since the mean air temperature at the buoy has a small diurnal variation, most of the variation in T_b - T_n results from the diurnal land-mass heating cycle in the tower network. A minimum in T_b - T_n corresponds to the time of maximum heating within the tower network.

From November to January, when sea breezes seldom occur, the time of maximum heating and peak wind speed are nearly coincident (Figure 3a). Also, the troughs and peaks along the curves are almost coincident,

suggesting that wind speeds increase in proportion to the daytime heating across the tower network. During the spring and summer months, a 3–4 hour separation occurs between the time of maximum heating (solid vertical lines in Figure 3b) and the time of maximum mean wind speed (dashed vertical lines in Figure 3b). These relationships suggest that synoptic gradients and vertical mixing through surface heating and destabilization drive the strength of winds during the winter months. Meanwhile, the delay in peak wind speeds during the spring and summer are consistent with the high frequency of sea breezes, caused by the temperature contrasts between the air over land and water. The sea breeze circulation strength peaks after the time of maximum contrast between the land-water temperatures. Convective outflows may play an additional minor role in the magnitude of the maximum mean wind speeds during the late afternoon hours in the summer months.

Contact Mr. Case at 321-853-8264 or case.jonathan@ensco.com or Dr. Bauman at 321-853-8202 or bauman.bill@ensco.com for more information on this work.

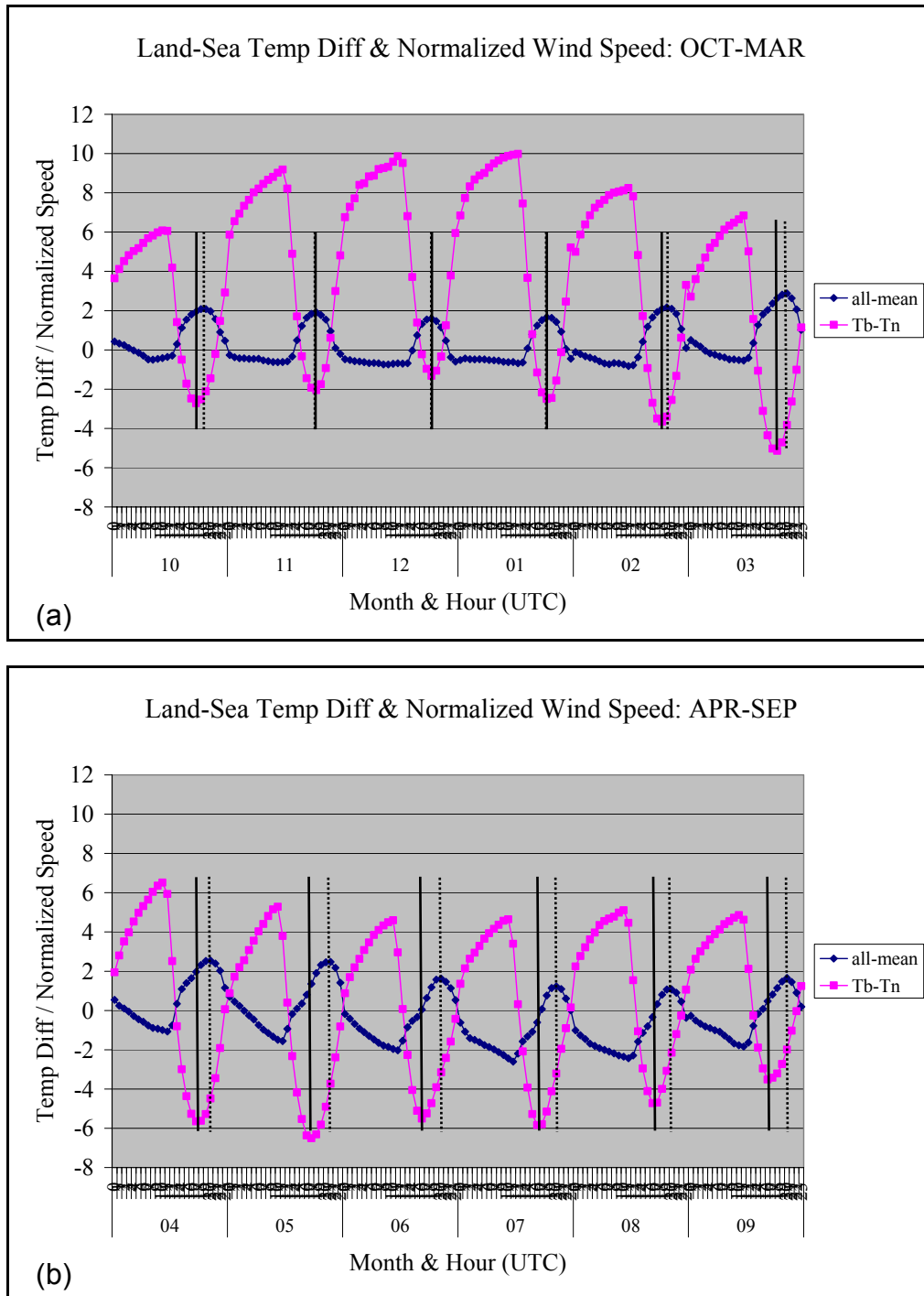


Figure 3. Plot of the hourly differences between the buoy and tower network mean 6-ft temperatures ($T_b - T_n$), and the hourly mean wind speed normalized by the monthly mean wind speed (all-mean), valid for the months of (a) October to March, and (b) April to September. Solid lines represent the time of minimum $T_b - T_n$ and dashed lines represent the time of the maximum mean wind speed. The hourly values by month are along the x-axis. The months are represented by their numerical value on the x-axis, and the individual hours in each month are difficult to discern because they are very close together on the axis.

Severe Weather Forecast Decision Aid (Mr. Wheeler and Dr. Bauman)

The 45 WS Commander's morning weather briefing includes an assessment of the likelihood of local convective severe weather for the day in order to enhance protection of personnel and material assets of the 45th Space Wing, CCAFS, and KSC. The severe weather elements produced by thunderstorms include tornadoes, wind gusts ≥ 50 kts, and/or hail with a diameter ≥ 0.75 in. Forecasting the occurrence and timing of these phenomena is challenging for 45 WS operational personnel. The AMU has been tasked with the creation of a new severe weather forecast decision aid, such as a flow chart or nomogram, to improve the various 45 WS severe weather watches and warnings. The tool will provide severe weather guidance for the day by 1100 UTC (0700 EDT).

Dr. Bauman expanded the AMU database of severe weather events in east-central Florida by $\sim 5\%$ using a software tool called *SeverePlot* (<http://www.spc.noaa.gov/software/svrplot2/>) from the National Weather Service (NWS) Storm Prediction Center (SPC). *SeverePlot* displays data in tabular format as well as in graphical format plotted on a map as shown in Figure 4. The addition of the SPC severe reports completed the exhaustive search for severe weather events for this task.

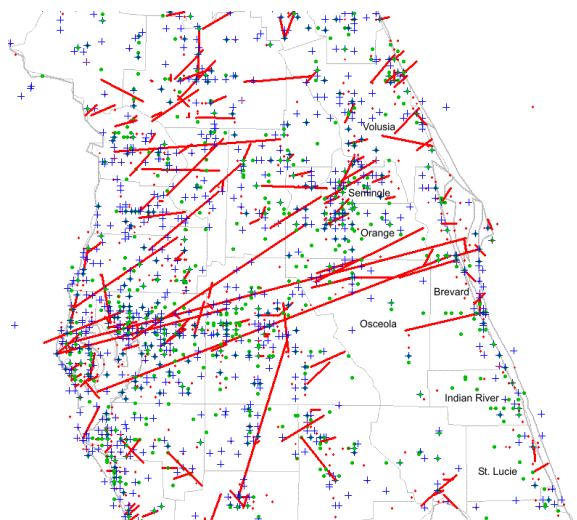


Figure 4. Severe storm reports from all months in the years 1960-2002 plotted using the *SeverePlot* software. It includes the reported tornado tracks (red lines), high winds (blue +) and hail (green dots).

Dr. Bauman analyzed the atmospheric stability indices and other parameters from the morning rawinsonde observation at XMR for all warm season days (May-September) from 1989-2003 and compared the indices to days with reported severe weather and days without reported severe weather. The distinction between the two is important because it is very possible there were days with severe weather occurring in east-central Florida but it was not observed and therefore not reported. The following indices were analyzed by Dr. Bauman, the first 4 of which are used by the 45 WS on their severe weather checklist:

- Lifted Index (LI)
- K-Index (KI)
- Total Totals (TT)
- Showalter Stability Index (SSI)
- Severe Weather Threat Index
- Thompson Index
- Cross Totals
- Convective Available Potential Energy (CAPE)
- CAPE (Maximum θ_e)
- CAPE (Forecast Maximum Temperature)
- Convective INhibition (CIN)
- Precipitable Water
- 500 mb Temperature
- Helicity

Figure 5 shows a scatter plot of the LI for days with reported severe weather and days without reported severe weather. The LI values are displayed on the y-axis and the x-axis represents the days in the period May-September 1989-2003, in chronological order. The days with reported severe weather are indicated by a red dot, those with no reported severe weather, a green dot. The "Low", "Medium", and "High" labels represent the 45 WS severe weather thresholds as found on their severe weather checklist. The days with reported severe events do not indicate a pattern consistent with the 45 WS severe weather threat levels. It appears that severe weather can occur with a similar frequency between LI values of 1 and -7. Furthermore, days with no reported severe weather display a similar pattern as days with reported severe weather. Figures 6-8 show similar scatter plots of the KI, TT, and SSI, respectively. Much like the LI in Figure 5, these indices do not show an obvious pattern to discern between severe and non-severe days.

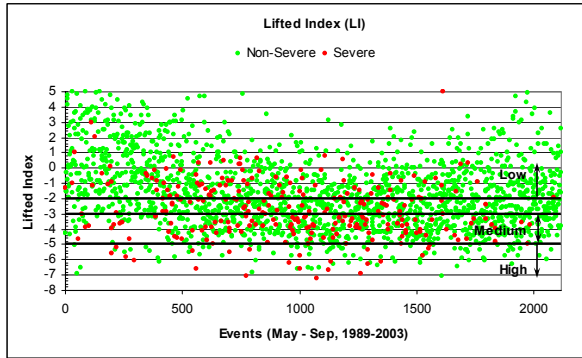


Figure 5. Scatter plot of Lifted Index values versus all thunderstorm days in May-September 1989-2003. Red dots indicate reported severe weather and green dots indicate no reported severe weather.

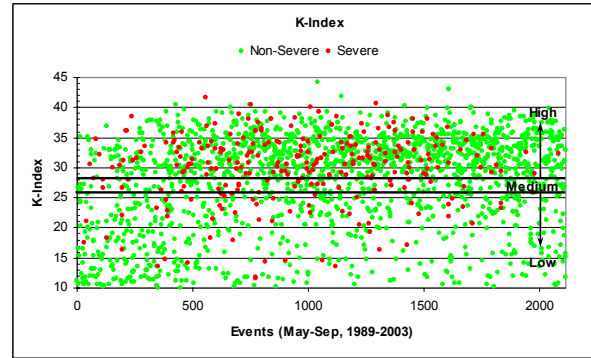


Figure 6. Scatter plot of K-Index values versus all thunderstorm days in May-September 1989-2003. Red dots indicate reported severe weather and green dots indicate no reported severe weather.

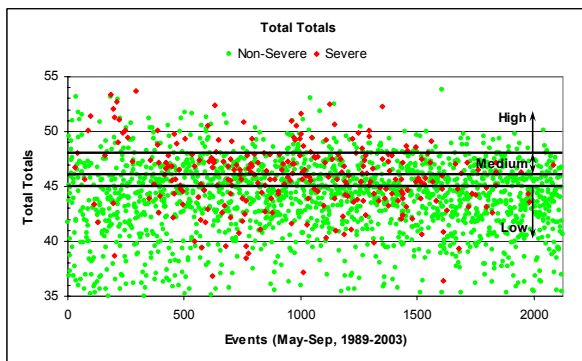


Figure 7. Scatter plot of Total Totals values versus all thunderstorm days in May-September 1989-2003. Red dots indicate reported severe weather and green dots indicate no reported severe weather.

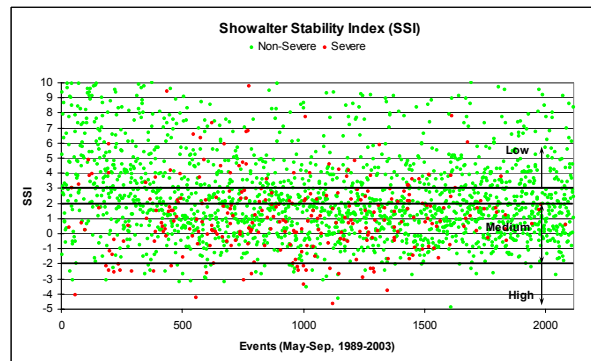


Figure 8. Scatter plot of Showalter Stability Index values versus all thunderstorm days in May-September 1989-2003. Red dots indicate reported severe weather and green dots indicate no reported severe weather.

When only days with severe wind reports are considered, KI appears to be a good predictor of the potential for severe winds. Figure 9 shows a scatter plot of 184 severe wind event days and their associated KI value. Of these events, 74% (137) had KI values at or above the 45 WS “High” threat level. This does not imply a severe wind event will occur when the KI is in the “High” region, but it does indicate a severe wind is much less likely when the KI values are in the “Medium” or “Low” ranges. The other three 45 WS indices (not shown) do not perform as well.

Mr. Wheeler completed an analysis of the synoptic features and dynamics for the days in the AMU database of severe weather events. Using archived surface analyses (Figure 10) and 300 mb analyses (Figure 11), he determined the locations of the surface ridge and upper level jet streak to include whether or not east-central Florida was under the influence of “no jet streak”, “upper level

divergence”, “jet streak overhead”, or “jet streak exit region”.

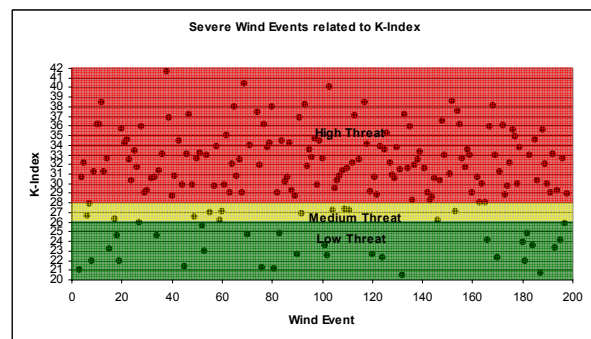


Figure 9. Scatter plots of K-Index values versus days on which severe wind events were reported. The red region represents the “High” threat values, the yellow region represents the “Medium” threat values and the green region represents the “Low” threat values.

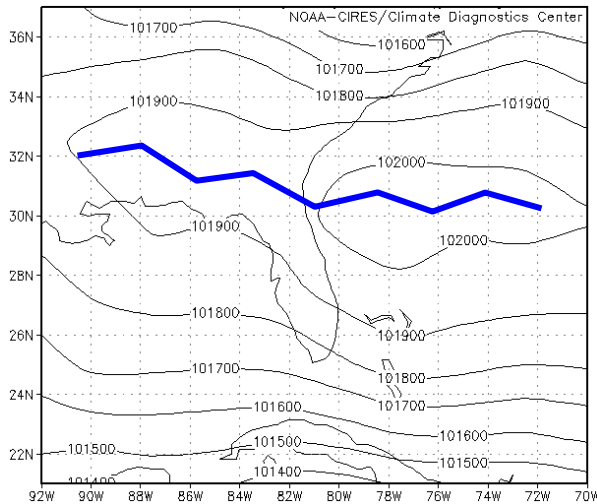


Figure 10. This is the 0000 UTC 12 May 2001 surface pressure analysis. It is an example of the surface pressure analyses used to determine surface ridge position. The ridge axis is highlighted by the blue line.

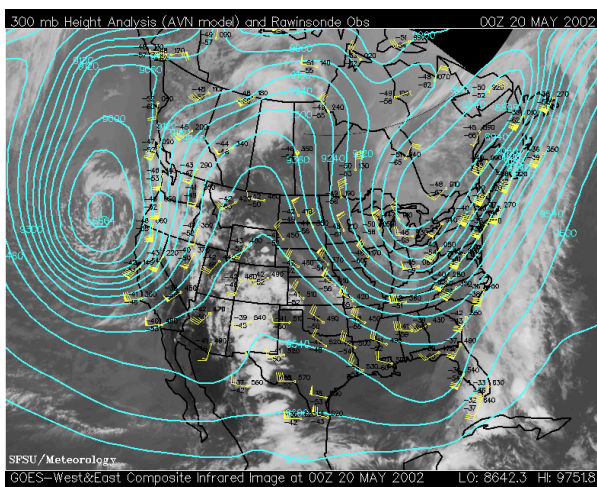


Figure 11. This is the 0000 UTC 20 May 2002 300 mb height and wind analysis. It is an example of analyses used to determine jet streak dynamics. The wind barbs are in yellow and the height contours in cyan.

In the surface pressure analysis, Mr. Wheeler found that the surface ridge was south of KSC/CCAFS on days with reported severe weather 60% of the time (Figure 12a) and split almost evenly between north, south, and no surface ridge for days with no reported severe weather (Figure 12b). His analysis of the upper-level jet streak revealed little difference in its position between severe (Figure 13a) and non-severe weather days (Figure 13b). Most of the time there was no jet streak to influence upper-level dynamics in both scenarios. There were 12% more divergent cases for the severe weather days

than non-severe, but the divergent cases still only accounted for one third of all severe days.

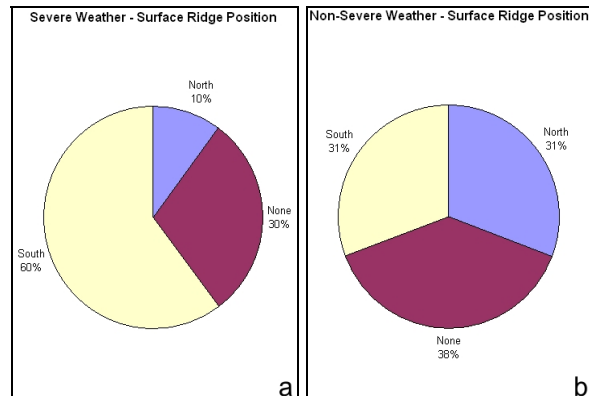


Figure 12. Pie charts showing the percentage of cases in which the surface ridge was north or south of KSC/CCAFS, or did not exist as a function of (a) severe days and (b) non-severe days.

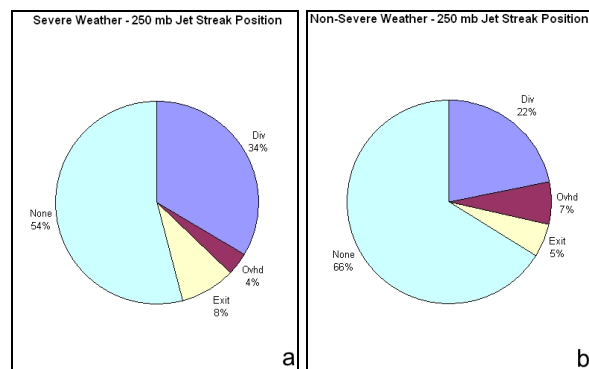


Figure 13. Pie charts showing the percentage of cases of the four different 300 mb jet streak positions as a function of (a) severe days and (b) non-severe days.

Currently, the subset of the database in which no severe weather was reported also includes days on which no thunderstorms occurred. Dr. Bauman and Mr. Wheeler will perform an analysis of the CGLSS data to differentiate thunderstorm days from non-thunderstorm days to determine if the stability indices can first be used as predictors of thunderstorm days and then further refined for use as severe weather predictors. They will also analyze severe weather days, non-severe thunderstorm days, and non-thunderstorm days based on the surface ridge position. Finally, the differences in stability indices from day-to-day will be calculated to look for stability trends as a severe weather predictor.

Contact Mr. Wheeler at 321-853-8205 or wheeler.mark@ensco.com, or Dr. Bauman at 321-853-8202 or bauman.bill@ensco.com for more information on this work.

Shuttle Ascent Camera Cloud Obstruction Forecast (Dr. Short and Mr. Lane)

Optical imaging of the Space Shuttle launch vehicle (hereafter the Shuttle) from ground-based and airborne cameras is susceptible to obstruction by clouds. The Columbia Accident Investigation Board (CAIB) recommended that the Shuttle ascent imaging network be upgraded to have the capability of providing at least three useful views of the Shuttle from lift-off to Solid Rocket Booster (SRB) separation. In response, the NASA/KSC Weather Office tasked the AMU to develop a model to forecast the probability that, at any time from launch to SRB separation, at least three of the Shuttle ascent imaging cameras will have a view of the Shuttle unobstructed by cloud. The resulting model was based on computer simulations of 1) idealized, random cloud coverage scenarios, 2) the optical lines-of-sight from cameras to the Shuttle using the camera network before and after upgrades for Return to Flight and 3) a Shuttle ascent trajectory for a launch from Pad 39B to the International Space Station (ISS).

The computer simulation model was used to estimate the probability that a network of cameras could obtain at least three simultaneous views of the Shuttle from lift-off to SRB separation in the presence of clouds. The model generated line-of-site (LOS) data for the camera network and Shuttle ascent trajectory, which were embedded in a three-dimensional (3-D) field of randomly distributed clouds. The LOS from each camera to the Shuttle was computed along its trajectory and cloud obscuration was noted as a binary variable, either obscured (1) or clear (0). The obscuration data were then analyzed to determine the fraction of time from liftoff to SRB separation that at least N simultaneous views of the Shuttle were obtained by the camera network, where N ranged from 2 to 6. A total of 1000 trials with randomly distributed clouds were analyzed for each of 19 different cloud scenarios. The cloud scenarios had defined cloud bases, tops and sizes, with cloud coverage ranging from clear (0/8) to overcast (8/8) in increments of 1/8.

Shuttle Ascent Imaging Network Before and After Upgrade

In response to the CAIB recommendation, the Intercenter Photo Working Group (IPWG) proposed several possible upgrades to the imaging network. These upgrades included additional long-range ground-based and airborne cameras. Figure 14 shows 11 ground-based, and

2 airborne long-range camera sites included in a proposed upgrade. Prior to the upgrade the network consisted of five long-range camera sites at Shiloh, Playalinda Beach, Universal Camera Site (UCS) 23, Cocoa Beach and Patrick Air Force Base (PAFB). The proposed upgrade initially involved dropping the PAFB site and adding ground based sites at Ponce Inlet, Apollo Beach, Launch Complex (LC) 46, UCS-11, UCS-3, and UCS-25, for a total of 10 ground-based long-range camera sites. The upgrade proposal also included airborne cameras to be located 15 n mi NW and SE of the SRB separation point, at 65 000 ft altitude. The IPWG recently considered an upgrade of the ground-based network with only 8 camera sites by dropping the Shiloh and UCS-25 sites, marked with open triangles in Figure 14.

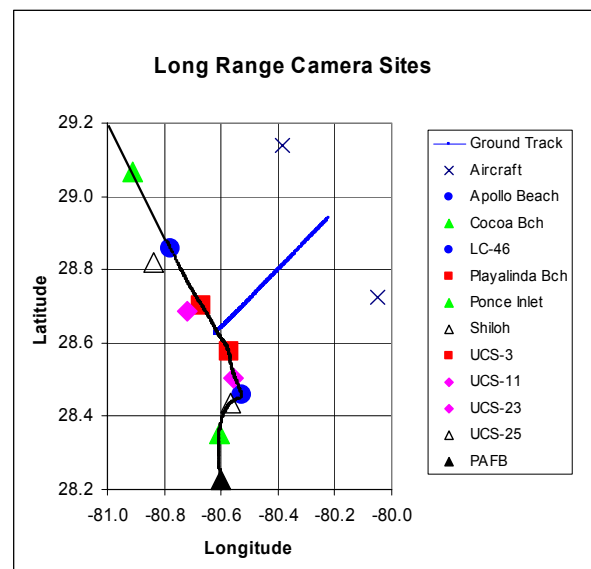


Figure 14. Locations of all pre- and proposed-upgrade long-range camera sites. The airborne cameras are at 65 000 ft 15 n mi NE and SW of the SRB separation point. The ground-track of a Shuttle ascent trajectory to the ISS from lift-off to SRB separation is shown by the solid line.

Performance Comparison between the Pre- and Post-Upgrade Camera Networks

Dr. Short completed a comparative analysis between the performance of the pre- and proposed-upgrade camera networks in their ability to provide three simultaneous views of the Shuttle before and after the network upgrade. He selected a cloud field that had 8000 ft bases and a 500 ft thickness. Cloud horizontal extents were 1, 4, and 8 n mi and cloud cover ranged from clear to overcast. Figure 15 shows the average percent of time from lift-off to SRB separation that the Shuttle

was viewable simultaneously by at least three cameras. The percent viewable time is 100% under clear conditions and decreases to 22% for overcast conditions because that is the amount of time it takes for the shuttle to reach cloud base and to be completely obscured from all the ground-based cameras. For this cloud scenario the medium and short-range cameras do not affect the results because their useful imagery is limited to the time from lift-off to when the Shuttle reaches an altitude of 7000 ft, which is below the chosen below cloud base.

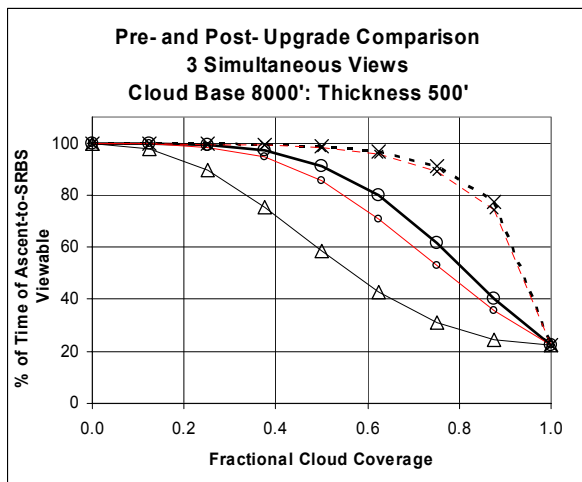


Figure 15. Fractional cloud coverage versus % of ascent-to-SRB separation time period that the Shuttle is viewable simultaneously by at least 3 cameras for several configurations of the camera network: Pre-upgrade (Δ), Post-upgrade with 8 ground-based long-range cameras (o), Post-upgrade with 10 ground-based long-range cameras (O), Post-upgrade with 8 ground-based and 2 airborne long-range cameras (x), and Post-upgrade with 10 ground-based and 2 airborne long-range cameras (X).

Figure 15 shows that as cloud cover was increased from clear to 0.5 coverage, the percent viewable time for the pre-upgrade network decreased to just under 60%, whereas the upgraded networks decreased more slowly to 85% or better. As cloud cover was increased from 0.5 up to 0.75, the percent viewable time decreased to less than 80% for all configurations, except those that included the airborne cameras. As cloud coverage approached overcast conditions, all network configurations rapidly converged to the 22% level.

Contact Dr. Short at 321-853-8105 or short.david@ensco.com, or Mr. Lane at 321-783-9735 Ext. 245 or lane.bob@ensco.com for more information on this work.

INSTRUMENTATION AND MEASUREMENT

I&M and RSA Support (Dr. Bauman and Mr. Wheeler)

Mr. Wheeler attended a RSA Technical Interchange Meeting at the Forecast Systems Lab (FSL) in Boulder, CO in June. Topics of discussion included the purchase of new computer modeling hardware, upgrade of all Linux operating systems, upgrade of the operational radar processing software, and upgrade of the Advanced Weather Interactive Processing System (AWIPS). Mr. Wheeler also attended an AWIPS system-level training session at FSL. Dr. Bauman and Mr. Wheeler attended a meeting at the NWS office in Melbourne FL (MLB) with representatives from the 45 WS. They discussed the NWS utilization of AWIPS and saw a demonstration of the Weather Event Simulator.

Anvil Transparency Relationship to Radar Reflectivity (Dr. Short and Mr. Wheeler)

Determining the transparency of anvil clouds is critical for the operational evaluation of FR and LCC. A non-transparent anvil that is attached to its parent thunderstorm is likely to be electrically charged and could subject a launch vehicle or landing Shuttle to a natural and/or triggered lightning strike. Forecasters currently rely on satellite observations, pilot reports and surface based observations to determine if anvil clouds are non-transparent, which would be a violation of LCC and FR if the flight path of a vehicle were to pass through such clouds. However, these types of cloud observations are not always available, depending on the location of the anvil clouds, the presence of other cloud layers and the time of day. The Weather Surveillance Radar 1988 Doppler (WSR-88D) at NWS MLB provides high-resolution cloud reflectivity information over the KSC/CCAFS area on a continuous basis. Routine products from the WSR-88D could be useful for determining anvil transparency and are available in real-time at SMG and the 45 WS Range Weather Operations. One of those products identified by SMG is the Layer Composite Reflectivity Maximum (LRM) High product, which determines the maximum reflectivity value in the 33 000 – 60 000 ft layer. The AMU was tasked to determine if the WSR-88D LRM High product would be useful in evaluating anvil transparency.

Dr. Short and Mr. Wheeler identified 45 case days during the warm season of 2003 (May – September) with thunderstorm anvil clouds over the KSC/CCAFS area. The anvils were clearly identifiable in visible and infrared satellite imagery and with the high cloud transparency remarks recorded by weather observers at the SLF weather station (KTTS). Of the 45 case days, 41 had LRM products available. On those 41 days a total of 313 daylight hourly observations of thunderstorm anvil clouds over KTTS were found with coincident LRM products and anvil transparency remarks.

The LRM Mid and High products from the WSR-88D for the 45 case days were requested from the National Climatic Data Center. The task originally called for an analysis of the LRM High product only based on previous experience that showed the movement of anvil clouds were highly correlated with the wind speed and direction in the layer between 30 000 and 45 000 ft (Short et al. 2004). Dr. Short and Mr. Wheeler decided to analyze the LRM Mid product, which displays the maximum reflectivity in the 24 000 – 33 000 ft level, because the anvil clouds sampled in the KSC/CCAFS area during the Airborne Field Mill program (Merceret and Christian 2000) were below 30 000 ft.

Dr. Short and Mr. Wheeler selected a 3 x 3 grid of LRM cells over KTTS (Figure 16) to match the area over KTTS monitored by the ground-based observers in their special effort to evaluate cloud transparency. The grid also takes into account navigation errors in the radar product due to variations in the refractive properties of the atmosphere from day-to-day. For each hourly KTTS observation with transparency remarks, the nine values of the LRM product within the 3 x 3 grid were recorded as integers, 0 for < 0 dBZ, 1 for 0-4 dBZ (blue), 2 for 5-17 dBZ (green), etc. The record of anvil transparency remarks were merged with the integer values for the LRM products and classified for a categorical analysis: The observer evaluation was classified as yes for opaque and no for transparent anvil clouds. The radar observation was classified as yes if any of the 9 cells had a value ≥ 0 and no if all of the 9 cells had a value < 0.

Table 1 shows a standard contingency table used for computing verification statistics. Categorical data (yes/no) is entered in a 2 x 2 table of counts of the four possible combinations

of “observed” and “forecast.” Namely, yes/yes (a), no/yes (b), yes/no (c), and no/no (d). In the analysis presented here the KTTS observations are the “observed” events and the LRM radar indications are the “forecast” events.

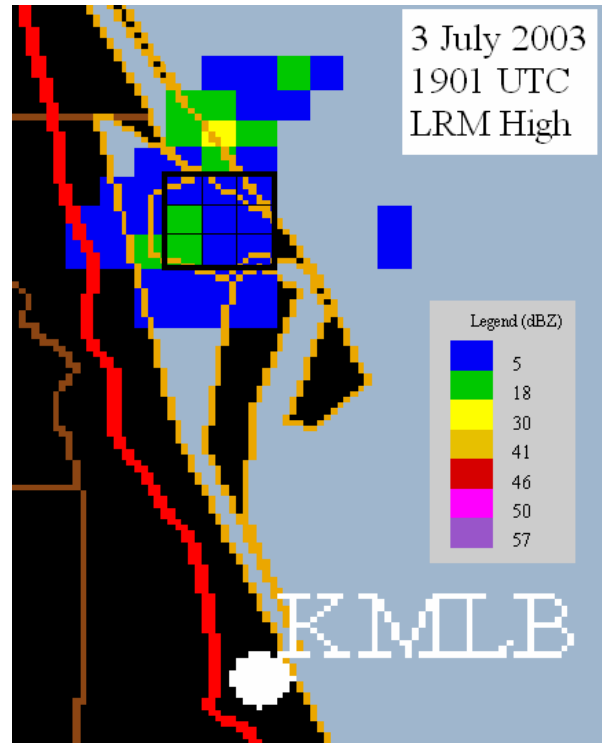


Figure 16. A portion of the LRM High image on 3 July 2003 at 1901 UTC. The 3 x 3 grid of cells over the northern portion of Merritt Island is over KTTS.

Table 1 also shows equations for the five measures of performance that will be assessed here: The False Alarm Rate (FAR), the Probability of Detection of yes (PODy), The Critical Success Index (CSI), the True Skill Statistic (TSS), and the Heidke Skill Score (HSS). FAR gives the proportion of yes forecasts that were incorrect. PODy gives the proportion of yes observations that were correctly forecast. CSI, also known as the Threat Score, gives the proportion of yes events that were either forecast or observed. TSS, also known as the Hanssen-Kuipers discrimination statistic, provides a measure of the forecast’s ability to discriminate between yes and no observations (Wilks 1995). A TSS of 1 indicates perfect forecasts, whereas random forecasts would result in a score of 0, and forecasts with skill less than random would give a negative TSS. The HSS gives the fraction of forecasts that are correct, corrected for the number expected to be correct by chance.

Dr. Short tested each LRM product individually and in combination with each other. Table 2 shows the contingency table comparing KTTS observations of anvil transparency with the combination of the LRM High and Mid products. This combination produced better performance than either the LRM High or Mid alone. The FAR was low at 10.1% because in approximately 9 out of 10 cases where LRM Mid or High values were

> 0 dBZ the observer reported non-transparent anvils. However, the PODy was only 49.7% meaning that the radar depicted only about half of the non-transparent cloud reports from the observer. As a consequence, the scores for the CSI, TSS and HSS were relatively low at 0.471, 0.532, and 0.437, respectively.

Table 1. A standard contingency table used for computing verification statistics and the equations for the measures of performance used in this report.

		Observation	
		Yes	No
Forecast	Yes	a	b
	No	c	d

FAR = $b/(a+b)$
 PODy = $a/(a+c)$
 CSI = $a/(a+b+c)$
 TSS = $(ad - bc)/[(a+b)(c+d)]$
 HSS = $[(a+d) - E]/(N-E)$
 where $N = a + b + c + d$
 and $E = [(a+c)(a+b)+(b+d)(c+d)]/N$

Table 2. Actual contingency table from the analysis of anvil transparency based on the KTTS observer's remarks and a combination of the LRM High and Mid product values. In this analysis the KTTS observations are the observed events and the LRM values are the forecast events.

		Observation	
		Yes	No
Forecast	Yes	80	9
	No	81	143

Using the above values for a, b, c, and d in the equations in Table 1, the LRM High and Mid products produce the following measures of performance:
 FAR = **10.1%** PODy = **49.7%** CSI = **0.471**
 TSS = **0.532** HSS = **0.437**

Theoretical Considerations

The transparency, or non-transparency, of a cloud depends on the optical extinction coefficient of its cloud particles and the thickness of the cloud. The cloud particles also determine the radar reflectivity. Therefore, there is a theoretical relationship between cloud transparency and radar reflectivity. Atlas et al. (1995) provide a theoretical approach for expressing the optical extinction coefficient of a cloud composed of ice crystals in terms of the radar reflectivity (Z) and D_0 , a characteristic size of the ice crystals.

The Atlas et al. (1995) approach can be combined with data from anvil clouds presented by McFarquhar and Heymsfield (1996) to infer that a realistic anvil cloud with a D_0 of 400 μ m and an anvil thickness of 10 000 ft would have an optical thickness of 3.93 if its radar reflectivity was

-5 dBZ. An optical thickness of 3.93 is very close to the threshold use for optical obscuration in visual range theory (Fleagle and Businger 1963). This indicates that opaque anvil clouds may not be detected by the LRM High and Mid products, if the anvil thickness was large enough and the reflectivity was below 0 dBZ.

A more detailed discussion of the tests Dr. Short conducted to estimate the relationships between radar reflectivity, optical extinction, optical depth, and the optical depth threshold is given in the final memorandum. These parameters could be used to make a distinction between transparent and non-transparent anvil clouds.

Conclusions

Dr. Short and Mr. Wheeler recommend limited use of the current LRM Mid and High products as indicators of non-transparent anvil clouds. The primary reason for the limited recommendation is that the LRM products had a low (49.7%) probability of detection of non-transparent anvil clouds. Nevertheless, the LRM Mid and High products had low false alarm rate at 10.1%, indicating that when the LRM High or Mid products showed maximum reflectivity values > 0 dBZ there was a high probability that the associated anvil cirrus clouds were non-transparent.

The reason for the discrepancy between the ground-based observer's assessment of cloud transparency and the radar reflectivity displayed in the LRM product appears to be in the nature of the LRM product. It provides the maximum radar reflectivity detected throughout the depth of a pre-defined layer but provides no information on the geometric thickness of cloud within the layer and has a lower cut-off at 0 dBZ. The lower cut-off and geometric thickness are important variables because theoretical calculations show that a cloud with a radar reflectivity below the cut-off (< 0 dBZ) could appear non-transparent to an observer if the cloud was sufficiently thick.

New software for creating a user-selectable LRM product from Level-II WSR-88D data may allow forecasters to change the lower cut-off to < 0 dBZ and for adjusting its height and depth levels. These options could be implemented at individual sites and may yield an LRM product capable of detecting a higher percentage of non-transparent anvil clouds. These options should be considered for future study.

For more information on this work or a copy of the memorandum, contact Dr. Short at 321-853-8105 or short.david@ensco.com, or Mr. Wheeler at 321-853-8205 or wheeler.mark@ensco.com.

MESOSCALE MODELING

User Control Interface for ADAS Data Ingest (Mr. Keen and Mr. Case)

The integrity of real-time, continuous diagnostic grids from the operational Advanced Regional Prediction System (ARPS) Data Analysis System (ADAS) has become very important, with a requirement to be operationally managed at the forecaster level. Forecasters at NWS MLB and SMG have the need for a user-friendly GUI in order to quickly and easily interact

with ADAS to maintain or improve the integrity of each 15-minute analysis cycle. The intent is to offer operational forecasters the means to manage and quality control the observational data streams ingested by ADAS without any prior expertise of ADAS required. Therefore, the AMU is tasked to develop a GUI tool to help forecasters manage the data sets assimilated into ADAS.

During this past quarter, Mr. Case met with Mr. Jeremy Keen of ENSCO, Inc., who will perform the GUI development. Mr. Case and Mr. Keen discussed the features that the GUI should have, and examined the scripts and input files associated with the current ADAS operational cycle at NWS MLB. They also met with personnel from NWS MLB to discuss the objectives and features of the ADAS control GUI. Mr. Keen developed some preliminary features based on files provided by Mr. Case, and began developing an interactive map that will allow users to quality control specific variables from selected surface stations across the Florida peninsula.

AMU CHIEF'S TECHNICAL ACTIVITIES (Dr. Merceret)

With assistance from Sharon Lewis at NCAR and Dr. Monte Bateman at Marshall Space Flight Center (MSFC), Dr. Merceret prepared four appendices to the Airborne Field Mill (ABFM) Program Final Report. These appendices cover the WSR-74C and WSR-88D weather radars as well as the Lightning Detection and Ranging and CGLSS systems used during the ABFM field program in 2000 and 2001. Principal investigator Dr. Jim Dye of NCAR is preparing the final report with input from all of the project scientists. Dr. Merceret also updated and tested a Visual Basic program that ingests and analyzes ABFM merged data files. The program produces statistics for weather phenomena such as anvil clouds and cloud-to-ground lightning. He also developed quantitative acceptance test criteria for the end-to-end meteorological acceptance test of the planned SLRSC modifications to the KSC 50-MHz wind profiler.

Dr. James Glover of Oral Roberts University arrived in May. He is a KSC Summer Fellow and will work on lightning cessation research under the AMU Visiting Scientist Program. He is conducting research on statistical forecasting of lightning cessation. Mr. Weems of the 45 WS provided CGLSS data from 51 well-defined and isolated storms within a 30 n mi radius of LC-40. Dr. Glover generated statistical best-fit curves for

decaying flash rates and identified an appropriate probability density model. He is developing a climatology and probability distribution for the time displacements between the last and second-to-last strikes of storms.

Ms. Angel Bennett, a junior in the Pennsylvania State University (PSU) meteorology program, arrived in June. She is a summer intern in PSU's KSC Internship Development Program. Her project involves statistical analysis of CGLSS data. Mr. Johnny Weems of the 45 WS provided 1994-2003 warm season CGLSS data that were within a 20 n mi radius of the Shuttle Vehicle Assembly Building (VAB). Ms. Bennett created charts and graphs to analyze lightning occurrence coincident with the Lericos et al. (2002) flow regimes. Her work will improve lightning probability forecasts used to plan movement of the Shuttle from the VAB to the launch pad, a very weather sensitive and lengthy process.

Ms. Jennifer Ward recently graduated from the University of Central Florida and is now employed by NASA in the KSC Weather Office. She participated in a work assignment from the NASA Accelerated Training Program by supporting the AMU. Ms. Ward's project included collecting central Florida census data to evaluate the effect of population density on the reported frequencies of severe weather events such as tornadoes, wind, and hail. The results of her work were used by the AMU in support of the Severe Weather Forecast Tool task.

AMU OPERATIONS

Mr. Wheeler worked with Dr. Merceret and NASA's procurement office to prioritize and clarify the AMU's purchase requests. Several of the requested items have been received.

Drs. Merceret and Bauman presented a paper titled "A Decade of Weather Technology Delivered to America's Space Program by the Applied Meteorology Unit" to the 41st Space Congress. The paper was co-authored with William Roeder (45 WS), Richard Lafosse (SMG), and David Sharp (NWS MLB).

Mr. Case traveled to Boulder, CO for two workshops: The First Joint Penn State Mesoscale

Model /Weather Research & Forecasting Model Workshop from 22-25 June, and the United States Weather Research Program's Community Meeting on Real-Time and Retrospective Mesoscale Objective Analysis from 29-30 June.

REFERENCES

- Atlas, D., S. Y. Matrosov, A. J. Heymsfield, M.D. Chou, and D. B. Wolff, 1995: Radar and radiation properties of ice clouds. *J. Appl. Meteor.*, 34, 2329-2345.
- Fleagle, R. G., and J. A. Businger, 1963: An Introduction to Atmospheric Physics. International Geophysics Series Volume 5. Academic Press, New York, 346 pp.
- Lericos, T. P., H. E. Fuelberg, A. I. Watson, and R. L. Holle, 2002: Warm season lightning distributions over the Florida Peninsula as related to synoptic patterns. *Wea. Forecasting*, 17, 83 – 98.
- McFarquhar, G. M., and A. J. Heymsfield, 1996: Microphysical characteristics of three anvils sampled during the Central Equatorial Pacific Experiment. *J. Atmos. Sci.*, 53, 2401-2423.
- Merceret, F. J., and H. Christian, 2000: KSC ABFM 2000 – A Field Program to Facilitate Safe Relaxation of the Lightning Launch Commit Criteria for the American Space Program. Preprints, 9th Conference on Aviation, Range, and Aerospace Meteorology, Orlando, FL, Amer. Meteor. Soc., 447-449.
- Short, D. A., J. E. Sardonía, W. C. Lambert, and M. M. Wheeler, 2004: Nowcasting thunderstorm anvil clouds over Kennedy Space Center and Cape Canaveral Air Force Station. *Wea. Forecasting*, 19, to appear.
- Wilks, D. S., 1995: *Statistical Methods in the Atmospheric Sciences*. Academic Press, Inc., San Diego, CA, 467 pp.
- WSR-88D Handbook, Volume 4, RPG, Revision No. 2, 2004: Operator Handbook, Guidance on Adaptable Parameters, Doppler Meteorological Radar, National Weather Service Radar Operations Center, 235 pp.

List of Acronyms

30 SW	30th Space Wing	LRM	Layered Reflectivity Maximum
30 WS	30th Weather Squadron	MIA	Miami FL 3-letter Identifier
45 RMS	45th Range Management Squadron	MSFC	Marshall Space Flight Center
45 OG	45th Operations Group	NASA	National Aeronautics and Space Administration
45 SW	45th Space Wing	NCAR	National Center for Atmospheric Research
45 SW/SE	45th Space Wing/Range Safety	NCDC	National Climatic Data Center
45 WS	45th Weather Squadron	NE	Northeast
ABFM	Airborne Field Mill	NOAA	National Oceanic and Atmospheric Administration
ADAS	ARPS Data Analysis System	NSSL	National Severe Storms Laboratory
AFSPC	Air Force Space Command	NW	Northwest
AFWA	Air Force Weather Agency	NWS MLB	National Weather Service in Melbourne, FL
AMU	Applied Meteorology Unit	PAFB	Patrick Air Force Base
ARPS	Advanced Regional Prediction System	PC	Personal Computer
AWIPS	Advanced Weather Interactive Processing System	PODy	Probability of Detection of Yes
BS	Brier Score	QC	Quality Control
CAIB	Columbia Accident Investigation Board	RSA	Range Standardization and Automation
CAPE	Convective Available Potential Energy	SE	Southeast
CCAFS	Cape Canaveral Air Force Station	SLF	Shuttle Landing Facility
CIN	Convective INhibition	SLRSC	Space Lift Range System Contract
CGLSS	Cloud-to-Ground Lightning Surveillance System	SMC	Space and Missile Center
CSI	Critical Success Index	SMG	Spaceflight Meteorology Group
CSR	Computer Sciences Raytheon	SPC	Storm Prediction Center
EDT	Eastern Daylight Time	SRB	Solid Rocket Booster
FAR	False Alarm Rate	SRH	NWS Southern Region Headquarters
FR	Flight Rules	SS	Brier Skill Score
FSL	Forecast Systems Laboratory	SSI	Showalter Stability Index
FSU	Florida State University	SW	Southwest
FY	Fiscal Year	TBW	Tampa FL 3-letter Identifier
GUI	Graphical User Interface	TSS	True Skill Statistic
HSS	Heidke Skill Score	TT	Total Totals
ISS	International Space Station	UCS	Universal Camera Site
JAX	Jacksonville FL 3-letter Identifier	USAF	United States Air Force
JSC	Johnson Space Center	UTC	Universal Coordinated Time
KI	K-Index	WSR-88D	Weather Surveillance Radar 1988 Doppler
KSC	Kennedy Space Center	WWW	World Wide Web
KTTS	Weather Station B Identifier	XMR	CCAFS Sounding Identifier
LCC	Launch Commit Criteria		
LI	Lifted Index		
LOS	Line-Of-Site		

Appendix A

AMU Project Schedule				
31 July 2004				
AMU Projects	Milestones	Scheduled Begin Date	Scheduled End Date	Notes/Status
Objective Lightning Probability Phase I	Literature review and data collection/QC	Feb 03	Jun 03	Completed
	Statistical formulation and method selection	Jun 03	Oct 03	Completed, but delayed due to errors found in COTS software
	Equation development, tests with verification data and other forecast methods	Aug 03	Nov 03	Delayed as above
	Develop operational products	Nov 03	Jan 04	Delayed as above
	Prepare products, final report for distribution	Jan 04	Mar 04	Delayed as above
Mesonet Temperature and Wind Climatology	Process data and calculate climatology of biases/deviations	Jul 03	Feb 04	Completed
	Develop tabular and geographical displays	Feb 04	Apr 04	Completed
	Final Report	Apr 04	Jun 04	Completed Draft
	Assistance in transitioning product into operations	Jul 04	Jul 04	On Schedule
Severe Weather Forecast Tool	Local and national NWS research, discussions with local weather offices on forecasting techniques	Apr 03	Sep 03	Completed
	Develop database, develop decision aid, fine tune	Oct 03	Apr 04	Delayed due to higher priority Shuttle Ascent Camera Cloud Obstruction Forecast Task
	Final report	May 04	Jun 04	Delayed as above
Expanded Statistics Towers Task for Edwards AFB and Northrup Strip	Deliver wind tower QC FORTRAN code to personnel at MSFC	Jun 04	Jun 04	Completed
	Deliver MS Excel file containing wind tower statistics GUI and associated VBA scripts to personnel at MSFC	Jun 04	Jun 04	Completed
	Provide consultation on QC code and Excel VBA scripts	Jun 04	Sep 04	On Schedule

AMU Project Schedule 31 July 2004				
AMU Projects	Milestones	Scheduled Begin Date	Scheduled End Date	Notes/Status
Shuttle Ascent Camera Cloud Obstruction Forecast	Develop 3-D random cloud model and calculate yes/no viewing conditions from optical sites for a shuttle ascent	Jan 04	Jan 04	Completed
	Analyze optical viewing conditions for representative cloud distributions and develop viewing probability tables	Feb 04	Feb 04	Completed
Shuttle Ascent Camera Cloud Obstruction Forecast (continued)	Memorandum	Feb 04	Jun 04	Delayed to provide support for Program Requirements Control Board Briefings
Anvil Transparency Relationship to Radar Reflectivity	Literature search and identification of days with anvil cloud over weather station B near the SLF	Nov 03	Dec 03	Completed
	Analysis of WSR-88D and satellite data for anvil days	Jan 04	May 04	Completed
	Memorandum	Jun 04	Jul 04	On Schedule
Mesoscale Model Phenomenological Verification Evaluation	Literature search for studies in which phenomenological or event-based verification methods have been developed	Jun 04	Jan 05	On Schedule
	Determine operational feasibility of techniques found in the literature	Jul 04	Jan 05	On Schedule
	Final Report	Jan 05	Mar 05	On Schedule
User Control Interface for ADAS Data Ingest	Develop control graphical user interface (GUI)	Apr 04	Jan 05	On Schedule
	Installation assistance and documentation	Jan 05	Mar 05	On Schedule

NOTICE

Mention of a copyrighted, trademarked, or proprietary product, service, or document does not constitute endorsement thereof by the author, ENSCO, Inc., the AMU, the National Aeronautics and Space Administration, or the United States Government. Any such mention is solely for the purpose of fully informing the reader of the resources used to conduct the work reported herein.

